Bulletin of the Seismological Society of America, Vol. 83, No. 6, pp. 1835–1854, December 1993

AMPLITUDES OF CORE WAVES NEAR THE *PKP* CAUSTIC, FROM NUCLEAR EXPLOSIONS IN THE SOUTH PACIFIC RECORDED AT THE "LABORATOIRE DE DÉTECTION ET GÉOPHYSIQUE" NETWORK, IN FRANCE

BY S. HOUARD, J. L. PLANTET, J. P. MASSOT AND H. C. NATAF

ABSTRACT

The purpose of this paper is 2-fold. It is first a continuation of the study of Massot and Rocard (1982) on the amplitude variations of the core waves near the *PKP* caustic, for French nuclear explosions in the South Pacific recorded on the LDG network in France. Taking advantage of a larger available data set, and using current methods to compute synthetic seismograms, such as the WKBJ method, we reinvestigate the core waves amplitude versus distance variation pattern derived by Massot and Rocard (1982). The second purpose is to give precise constraints on the PKP caustic phenomenon, using waveform and amplitude comparisons between data and synthetics. WKBJ synthetics are computed for several global spherical Earth models. Recent models with a D″ discontinuity, or a low velocity gradient at the top and the bottom of the liquid core are also tested. Our computations do not support the highly variable amplitude versus distance profile of Massot and Rocard, which displays a major peak at 145.6° and many secondary interference fringes. Between 142° and 147°, the theoretical amplitude variations we have calculated are dominated by the large *PKP* caustic peak, and only modulated by the simultaneous arrival of the *PKIKP* wave near 145°. Using a data set of 17 nuclear explosions, we have measured relative amplitudes as a function of distance, in the 142° to 147° distance range, and analyzed the waveform variations. Our observations (amplitudes and waveforms) are well modeled by the 1066B model of Gilbert and Dziewonski (1975). The agreement on amplitude variations is still good for models PREM (Dziewonski and Anderson, 1981) and IASP91 (Kennett and Engdahl, 1991). Accurate quantitative constraints are derived on the *PKP* caustic, among which the position of the *B* caustic point (144.5° ± 0.5°) for the mean 296° Mururoa-LDG network azimuth. This location depends, as a whole, on the depth of the core-mantle boundary, and on the velocity gradients in the mantle and in outermost core. Although the depth of the core-mantle boundary, and the existence of a discontinuity at the top of *D″* can slightly affect the position of the *B* caustic point, the focusing effect at the PKP caustic is rather a global derivation of the models.

INTRODUCTION

Global spherical Earth models like PREM (Dziewonski and Anderson, 1981) or IASP91 (Kennett and Engdahl, 1991) represent essential tools for a travel-time, waveform, or amplitude analysis of seismic signals. Although they are a valuable starting base, their structure is sometimes inaccurate, especially near discontinuities. Many studies support the existence of a discontinuity at the top of the D″ layer at the base of the mantle (Lay and Helmberger, 1983; Baumgardt, 1989; Weber and Davis, 1990; Young and Lay, 1990; Gaherty and Lay, 1991; Weber, 1992; Houard and Nataf, 1992), a region which has long been recognized as rather anomalous and heterogeneous (Gutenberg, 1914; Bullen, 1949; Haddon and Cleary, 1974). Song and Helmberger (1993) recently investi-

gated the effect of the D″ structure on the *PKP* phases. The structure of the outermost core has been revised too, using *S* and *SmKS* waves (Choy, 1977; Lay and Young, 1990, Souriau and Poupinet, 1991). A small decrease of the *P* velocity is proposed, compared to PREM, and the existence of a stably-stratified chemical boundary layer is suggested (Lay and Young, 1990). The inner/outer core transition zone has also been widely investigated (Choy and Cormier, 1983; Cummins and Johnson, 1988; Souriau and Poupinet, 1991). The PREM structure is proved inaccurate to model the $PKP_{(BC+Cdiff)}$ propagation branch correctly (Choy and Cormier, 1983; Nakanishi, 1990), and lower *P* velocities are preferred at the base of the liquid core, supporting the existence of a stable stratification, related to the crystallization of the inner core (Souriau and Poupinet, 1991).

The study of these transition zones give interesting constraints on local zones of the Earth. The *PKP* caustic phenomenon gives a rather global constraint on the structure of the Earth because the *P*-velocity distributions in the mantle and outermost core, and the depth of the core-mantle boundary all play a role in this focusing effect. The rapid variation with distance of the core phases waveforms and amplitudes near the caustic provides a very sensitive test for global or locally revised models of the Earth.

Whereas many studies have been dedicated to the core/mantle and outer core/inner core transition zones, where important physical processes, like chemical differentiation or crystallization are expected, few studies have focused on the *PKP* caustic specifically. Jeffreys (1939) was the first to study it in a seismological context. Müller (1973) studied the amplitudes of the core waves to infer the structure of the outer and inner core, but he used long-period data. Of course, the *PKP* caustic is a classical candidate for checking computational methods of synthetic seismograms (Chapman and Orcutt, 1985), but comparisons of short-period data and synthetics have rarely been carried out. Massot and Rocard (1982), using two early Mururoa nuclear blasts recorded on the LDG

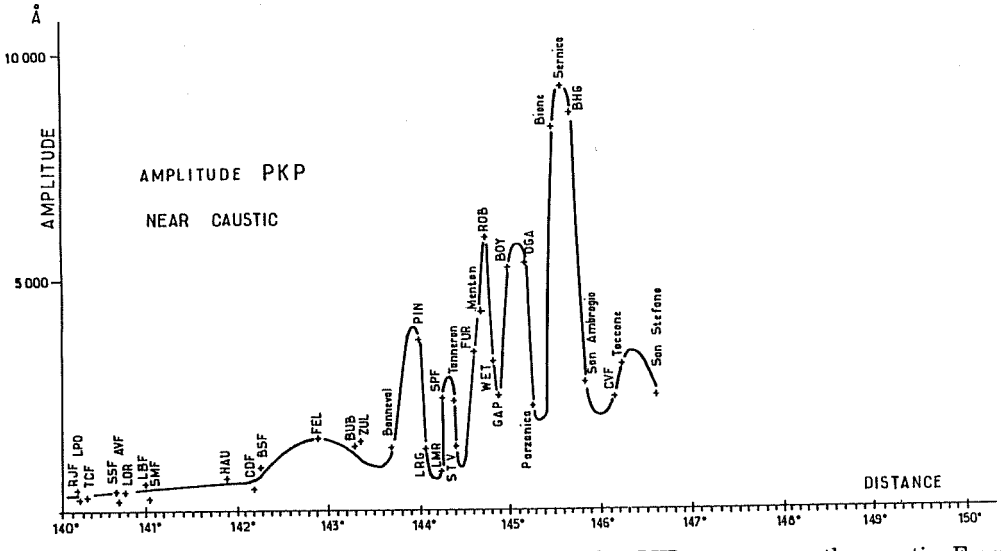

FIG. 1. Absolute amplitude versus distance plot for the *PKP* waves near the caustic. From Massot and Rocard (1982).

network and on mobile stations in Europe, derived a highly variable interpolated amplitude curve in the 140° to 147° distance range (Fig. 1). The amplitude variations were dominated by a major peak at 145.6°, and displayed many secondary interference fringes, some of them as thin as 0.3°. Because it is a rather spectacular result, we propose to reexamine the subject, using new data and more recent tools to compute the synthetic signals.

A precise study of the *PKP* caustic requires short-period data recorded on a large aperture, but rather dense seismic network. A large station density allows, to a certain extent, placement of bounds on the short-period amplitude scatter, and a large aperture is necessary to cover the whole caustic. The advantage of using explosions results from the exact knowledge of the origin time and geographical coordinates of the source, and thus from an exact knowledge of the epicentral distances and travel times. This is a valuable point, given the high variability of the waveforms and amplitudes of the signals near the caustic. Moreover, the source history parameters are well constrained, so that realistic synthetic sources can be constructed. Finally, unlike American, Chinese, or Russian test site explosions, the Mururoa explosions can generate core waves in the *PKP* caustic distance range that can be recorded on many seismic networks.

The LDG Network

The LDG network is run by the "Laboratoire de Détection et Géophysique" of the French nuclear agency (CEA). First installed around 1960, it provides digital data from about 30 stations since 1974 (Massinon & Plantet, 1976). Figure 2 shows the location of the stations. Most sites are on crystalline bedrock, and are equipped with the same vertical short-period seismograph. The total displacement response of the instrument is inserted at the *top right* of Figure 2. We give for comparison the short-period WWSSN instrument response. All data are telemetered in real time to LDG data center, with a sampling rate of 50 Hz. Epicentral distance circles centered on the Mururoa Atoll are also displayed in Figure 2, every 1°. Although the LDG network is rather well suited for this study, one can notice the absence of stations near 145° (where the theoretical calculations expect the greatest amplitudes), and beyond 146.5°.

Synthetic Seismograms

Synthetic seismograms are very helpful in the analysis of the core phases waveform and amplitude variations in the distance range investigated. In this distance range, the main contributions to vertical component seismograms result from the *PKP*, *PKIKP*, *PKiKP* (reflected from the upper side of the inner core boundary), and *PKIIKP* (reflected underneath the inner core boundary) arrivals. The raypaths of these waves are shown in Figure 3a, for a surface source and for a distance of propagation of 148°. Their hodochrones are displayed in Figure 3b, for model 1066B (Gilbert and Dziewonski, 1975). Note the position of the *C* diffraction point and of the *B* caustic point, where the *PKIKP* and the two *PKP*-wave arrivals are very close in time.

To compute realistic synthetic seismograms, we use the WKBJ method (Chapman, 1976, 1978; Dey-Sarkar and Chapman, 1978; Chapman and Orcutt, 1985). This method is based on a high-frequency approximation which makes of it a generalized ray-theory. The WKBJ method is well suited to model the

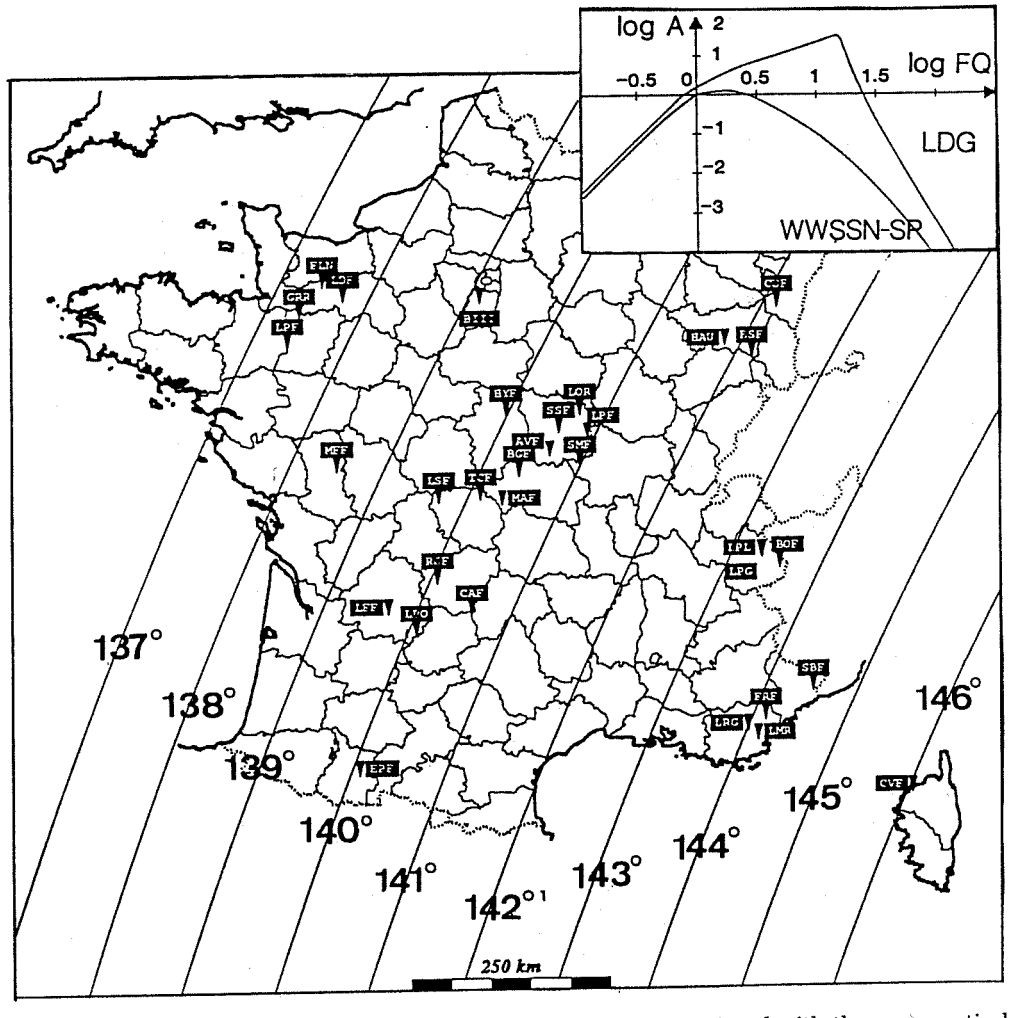

FIG. 2. Map of the French *LDG* network. All the stations are equipped with the same vertical short-period seismograph. Also plotted, every 1°: epicentral distance circles centered on the Mururoa atoll. The LDG instrumental displacement response is displayed in the insert (*top right*). It is compared with that of the WWSSN short-period response. Note that the maximum of sensitivity around 12 Hz.

short-period data of the LDG network. It is also well adapted to this study, for which only a small range of ray parameters has to be taken into account. The WKBJ method is valid at the *PKP* caustic: the integral over slowness is then evaluated by a third-order saddle point method, and is reduced to the Airy function (Chapman and Orcutt, 1985). The WKBJ theory is inaccurate for waves that graze the Earth's interfaces (Richards, 1976). This is clearly not the case for the PKP waves near the caustic (see raypaths in Fig. 3a). Nevertheless, we have checked our WKBJ code against the reflectivity algorithm (Kennett, 1983). The agreement between the two methods is very good for core waves computations, in the 140° to 150° distance range, both on travel times and waveforms. This gives us additional confidence in the reliability of the WKBJ method in the present study.

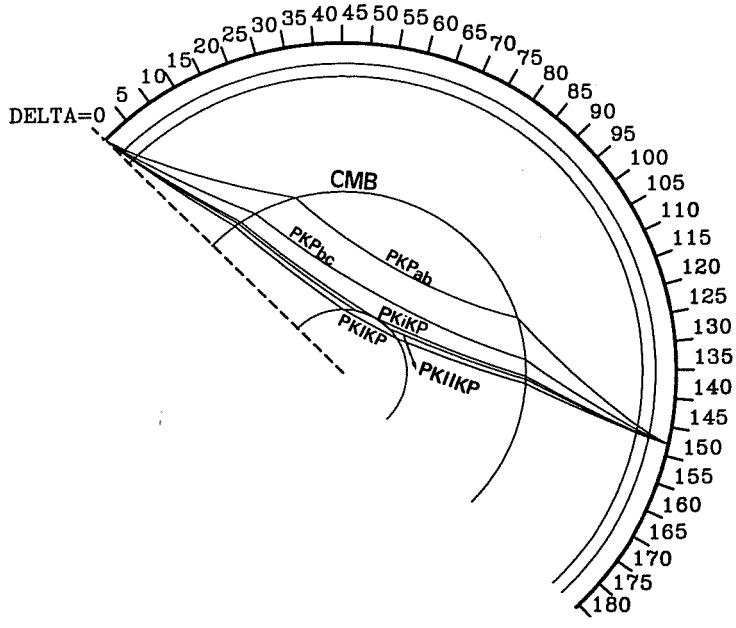

(a)

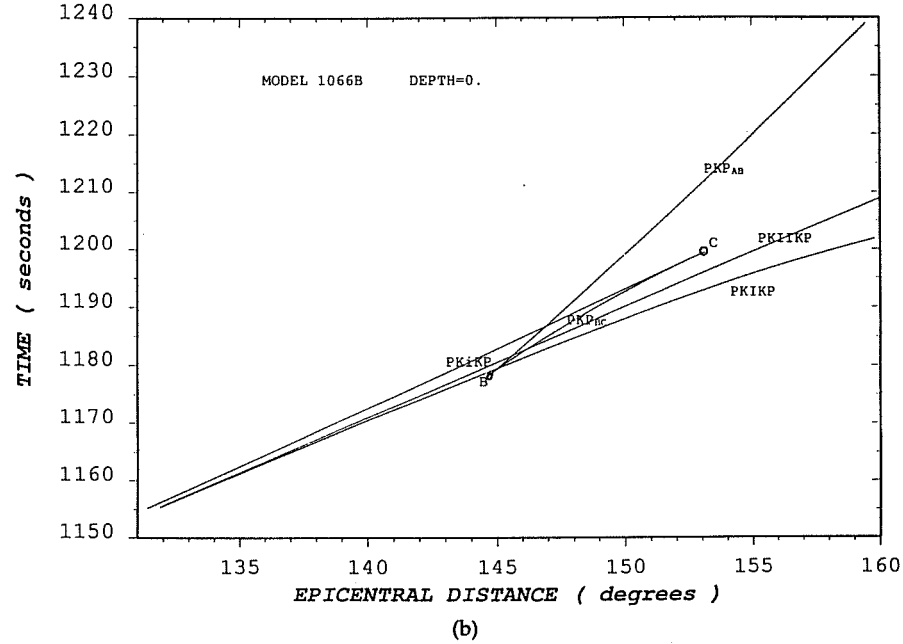

(b)

FIG. 3. (a) Raypaths of *PKIKP*, *PKIIKP*, *PKiKP*, PKP_{AB}, and PKP_{BC} waves computed at a distance of 148°, using the spherical IASP91 Earth model and a surface source. Note that the *PKP* waves do not sample the base of the outer core.

(b) Travel times curves of the core waves for model 1066B and for a surface source. Note the *PKP* *B* caustic point, where the PKP_{AB} and PKP_{BC} branches coalesce, and the *C* diffraction point, where the PKP_{BC} branch is diffracted on the outer core/inner core boundary.

The individual amplitude versus distance variations of the major core waves are plotted in Figure 4, computed for the 1066B model (Gilbert and Dziewonski, 1975). The *PKIIKP* amplitude is about ten times smaller than that of *PKIKP*, in the 140° to 147° distance range. Its contribution to realistic synthetic seismograms is minor, as well as the one of the higher order *PKnIKP* ($n > 2$) inner core reflections, and will not be computed. The contribution of the *PKIKP* wave is about half that of *PKiKP* in the 140° to 147° distance range. Its contribution to the waveforms of the synthetic signals is thus not negligible. However, its contribution to the maximum amplitude of the synthetics (see the "Amplitude Comparisons" section) is minor. Note the smooth decrease with distance of the *PKiKP* amplitude and the very smooth increase for *PKIKP*.

The amplitudes of the PKP_{AB} and PKP_{BC} branches show large and rapid variations between 140° and 147°. They both display a peak near 145° to 146°, due to the focusing effect at the caustic. Note that the *B* caustic point (Fig. 3b) is located about 1° shorter in distance than the top of the peak; the hodochrones are calculated using the geometrical ray theory, which is valid in the limit of infinite frequencies. Away from the caustic, the PKP_{AB} amplitude shows a rapid decrease, whereas the PKP_{BC} amplitude is almost constant up to 150°. Indeed,

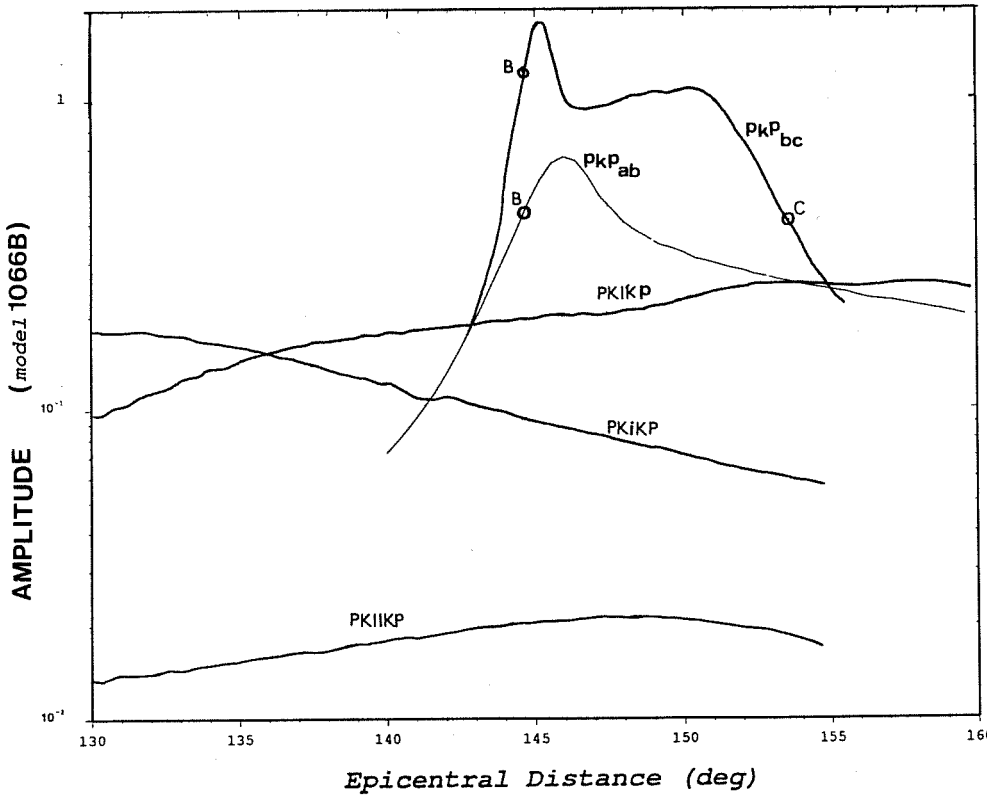

FIG. 4. *PKIKP*, *PKIIKP*, *PKiKP*, PKP_{AB}, and PKP_{BC} amplitude versus epicentral distance curves, for model 1066B. The amplitudes are the maximum amplitudes of synthetic seismograms computed using the WKBJ method. The anelasticity of the Earth, the LDG instrument response, and an explosive source time history are included. *B* and *C* points are indicated by circles. Theoretical amplitudes are no longer correct for PKP_{BC} waves (see text) beyond the *C* diffraction point. *PKP* amplitudes are not calculated below 140°.

theory shows that the PKP_{AB} and PKP_{BC} waves can respectively be considered as a maximum and as a minimum of the generalized travel-time function used in the WKBJ method (Dey-Sarkar and Chapman, 1978). The slight depression observed in the PKP_{BC} amplitude curve near 148° is more or less pronounced, depending on the Earth model considered. This feature is found to be sensitive to a change of velocity gradients at the bottom of the outer core (Houard *et al.*, 1991).

Because the wave grazes the inner core boundary, the PKP_{BC} amplitudes computed beyond the C diffraction point distance, at 153°, are no longer accurate as noted earlier. The amplitudes of diffracted waves are indeed overestimated in the far shadow (Chapman and Orcutt, 1985).

The *PKIKP*, *PKiKP*, PKP_{BC}, and PKP_{AB} waves all contribute to the construction of realistic synthetic signals. Because these waves can interfere with each other, in the 140° to 147° distance range, special care is needed concerning (1) the treatment of the Earth's attenuation, and (2) the computation of an explosive source time-history.

Anelastic Attenuation

We include attenuation effects in the Earth using an anelastic model. The $Q(r)$ model used is the one of PREM (Dziewonski and Anderson, 1981). However, the $Q(r)$ model of Cormier (1981) in the inner core is tested too, in the "Amplitude Comparisons" section. The intrinsic WKBJ algorithm works for a purely elastic Earth. It is possible, however, to take the attenuation into account, by convolving the WKBJ displacement with a causal dispersive operator (using t^* functions) standing outside of the integration step (Chapman *et al.*, 1988). For the waveform comparisons between data and synthetics, the t^* function used is that of the *PKIKP* wave. For the finer amplitude computations, each wave is computed separately, using the corresponding t^* function.

Source Time History

Explosive source time-functions have been widely investigated for the last two or three decades, and many synthetic source functions have been proposed. Their advantage over earthquake sources is their rather short duration and waveform stability from one blast to another. We use the Müller–Murphy (1971) source time-function, with appropriate medium parameters for the Mururoa test site. Surface reflections have to be taken into account. Instead of including them as supplementary rays in the WKBJ computations, we include them more simply via parameterized reflection and phase delay coefficients into the Müller-Murphy source, which is reasonable given the very small differences in ray parameter for the direct rays.

The realistic synthetic seismograms of the following sections include thus a convolution with (1) the LDG instrumental response, (2) a causal attenuation operator and (3) a Müller-Murphy source time-function.

Waveform Analysis

Considering the small magnitude of the events (Table 1), the waveform comparisons with the synthetic signals are carried out with stacked seismograms that result, for each LDG station, from the summation of several appropriate events. We expect thus the "stacked" event to display coherent features, more appropriate for a comparison with synthetic signals. For this stacking, we

TABLE 1

LIST OF EVENTS. THE EPICENTER PARAMETERS ARE FROM U.S.G.S. MONTHLY P.D.E. BULLETINS.

Date	h:m:s	lat (°)	long (°)	m_b
1983 04 19	18:52:58.4	21.847S	138.906W	5.6
1983 05 25	17:30:58.2	21.895S	139.918W	5.9
1984 05 12	17:30:58.3	21.852S	138.961W	5.7
1984 11 02	20:44:58.5	21.883S	139.048W	5.7
1984 12 06	17:28:58.6	21.848S	138.913W	5.6
1985 05 08	20:27:58.8	21.823S	138.048W	5.7
1985 11 26	17:41:58.4	21.867S	138.929W	5.8
1987 10 23	16:49:58.7	21.822S	139.029W	5.5
1987 11 19	16:30:58.3	21.904S	138.995W	5.9
1988 05 11	16:59:58.3	21.867S	139.072W	5.5
1988 05 25	17:00:58.4	21.903S	139.009W	5.6
1988 11 30	17:54:57.9	22.244S	138.836W	5.5
1989 06 10	17:29:58.1	22.252S	138.734W	5.5
1989 10 24	16:29:58.1	21.908S	138.977W	5.4
1989 11 27	16:59:58.0	22.276S	138.836W	5.6
1990 11 14	18:11:58.0	22.258S	138.805W	5.5
1991 05 29	18:59:58.2	22.256S	138.794W	5.5
*1985 09 11	17:47:36.0	15.388S	173.535W	5.8

*Samoa Island earthquake.

use a subset of eight Mururoa events that are carefully chosen. They are well distributed around a mean magnitude, so that the summation yields true mean waveform features. The change of epicenter location from one blast to another involves epicentral distance shifts less than 0.1°. For each station, the eight individual seismograms are summed, using a 2.2 sec/deg slowness. Assuming a mean 3.5 sec/deg slowness for the *PKP* wave near the caustic, a maximum phase shift of 0.1 sec is produced in the stacking procedure, which is small compared to the mean 1 sec period of the signals.

The stacked signals are displayed in Figure 5b, along with the theoretical travel time curves computed for model 1066B. The station corrections derived for the LDG stations, by Dziewonski and Anderson (1983), using *P* waves, have been applied for the data. A mean LDG network/Mururoa backazimuth is taken for the azimuthal dependence; coherent (upon stacking) energy arrivals are visible, between 137° and 143°, before the theoretical *PKIKP* arrival. The waveform of these precursors is highly variable, from one station to another. The maximum amplitude of these wave trains increases with epicentral distance, between 137° and 142°, and is even larger than that of the *PKIKP* wave at the HAU and BSF station. As distance increases, the difference of travel times between the first precursor onset and the *PKIKP* arrival decreases, and the precursors are no longer visible beyond 144°. Such precursors to the *PKIKP* wave have been widely reported in the literature, in this distance range. Haddon (1972) first proposed a comprehensive interpretation of the precursors as *PKP* waves scattered by a random distribution of small-scale heterogeneities within the D″ layer at the base of the mantle. Since then, the scattering interpretation has received considerable support (Haddon and Cleary, 1974; Husebye *et al.*, 1976; Bataille and Flatté, 1988). Using theoretical calculations

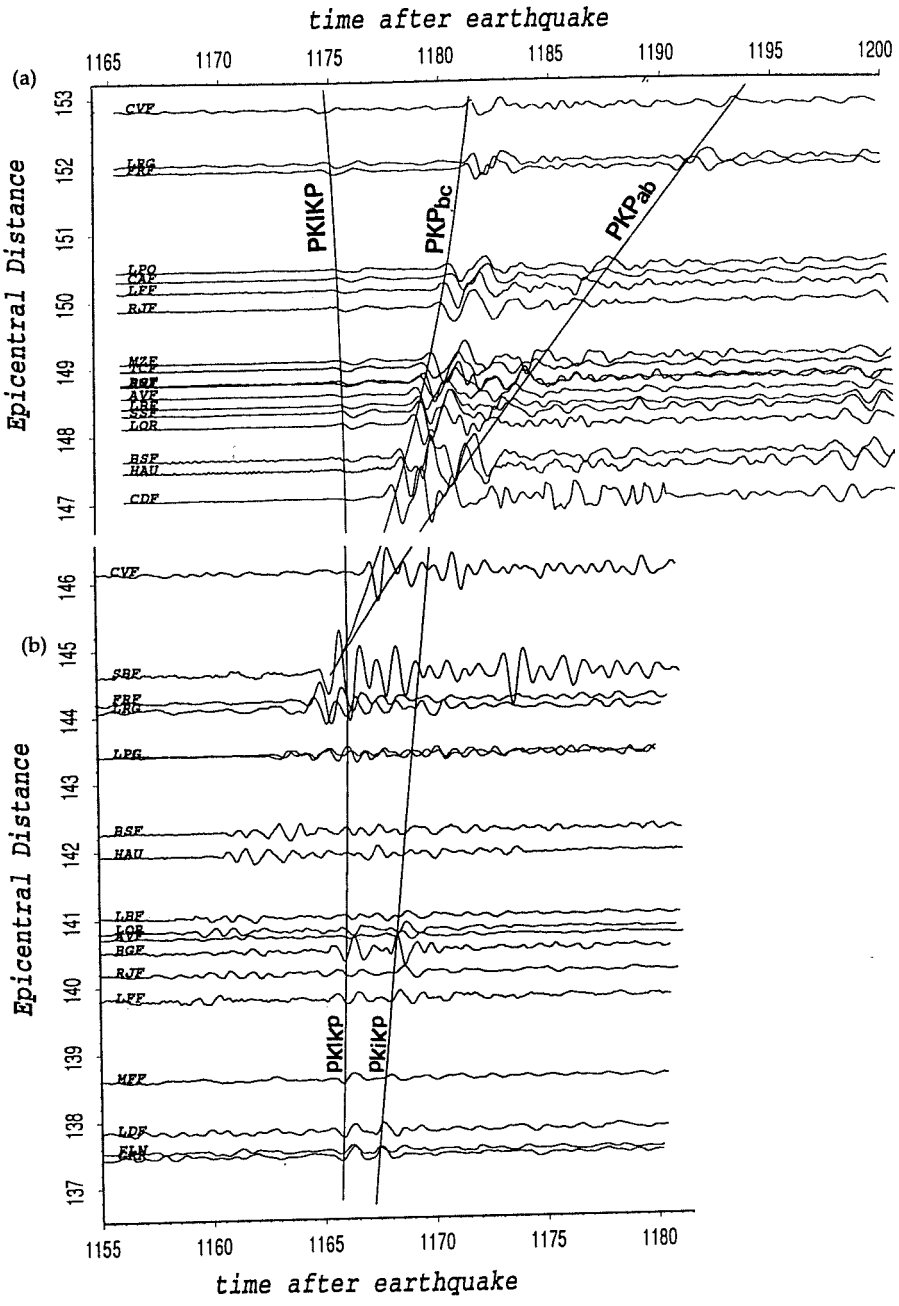

FIG. 5. (a) Record section for a 68.3 km deep Samoa Island earthquake recorded on the LDG network. Theoretical travel-time curves computed for *model 1066B* have been superimposed on it. A global 1.5 sec shift has been applied, for the theoretical *PKIKP* travel time to match the *PKIKP* onset in the data.

(b) Stacked seismograms of eight selected Mururoa explosions. Note the existence of energetic *PKIKP* precursors between 137 and 142°, and the large amplitude increase in the 144 to 146° range.

For both panels seismograms have been time-shifted using a 1.75 sec/deg slowness, and times apply to the station closest to the epicenter. The same scale is used for both panels. Note that the theoretical *PKP* travel times computed for the upper panel prolongate exactly into those computed for the *bottom* panel.

based on a first-order scattering integral, these authors have shown that the scattering mechanism accounts for most of the features of the *PKIKP* precursors (travel times, range of slownesses and azimuth deviations, amplitude variations, etc.) observed on seismic arrays. On the contrary, many of these features, such as azimuthal deviation from the great circle azimuth, are not explained if a sharp reflecting discontinuity is introduced at the base of the outer core (Bertrand and Clowes, 1974; Ergin, 1967, 1974).

Between 140° and 142°, the mean slowness of the maxima of these precursors is approximately 3 sec/deg (Fig. 5b), which is close to a direct *PKP* wave slowness near the caustic. Because the amplitude of the precursors is rather large at stations HAU and BSF at 142°, one may want to interpret them as *PKP* waves within the caustic geometrical shadow zone. However, only an Earth model with a *B* caustic point computed around 143° can produce so large *PKP* amplitudes at distances as short as 142°; this is illustrated in Figure 6, where WKBJ synthetics have been calculated for four global Earth models, at the epicentral distances spanned by the data. If the model derived by Anderson and Hart (1976) indeed produces large *PKP* amplitudes around 142° (Fig. 6, *bottom right* panel), the amplitudes are much too large in the 143° to 144° distance range to fit the data, and the synthetic waveforms are in strong disagreement with the data waveforms (Fig. 5b).

The precursors to the *PKIKP* wave observed on Figure 5b between 137° and 142°, are thus bound to be *PKP* waves scattered on the mantle-core boundary. Our waveform and amplitude analysis will now focus on direct core phase features only because our main interest in the study of the *PKP* caustic phenomenon itself.

The best agreement between the observed and synthetic waveforms is found for the 1066B model (Gilbert and Dziewonski, 1975). The synthetic *PKIKP* and *PKiKP* waveforms (Fig. 6, *top right*) are very close to the ones observed on the stacked seismograms, as well as their arrival times and move-out throughout the network. The 1066B synthetic calculations are also in good agreement with the large amplitude variations observed on the stacked signals (Fig. 5b) between 144° and 146°. The *PKP* wave becomes visible at LPL and LPG stations at 143.5° on both synthetics and data. The rapid increase of amplitude due to the caustic effect is well synthesized. Note the agreement between synthetic (Fig. 6, *top right* panel) and recorded (Fig. 5b) waveforms at station SBF, for the first seconds of signal. Two large secondary arrivals are visible, 2 to 3 sec and 7 to 8 sec after the first arrivals. However, such features are often observed at this station, using direct *P* records in the 80° to 90° distance range, and may thus be attributed to crustal effects beneath the station. More generally, stations in the Alps (LPL, LPG) and Provence (LMR, LRG, FRF, SBF) often display complex responses, probably due to the complexity of the crust beneath them. However, it was not possible to model them correctly for *P* waves because the secondary arrivals display important amplitude variations with the azimuth and distance (Fig. 6b [S. Houard and H.-C. Nataf, unpublished manuscript]).

The agreement on the *PKP* waveform is also good at station CVF (146.2°), located in Corsica. However, note the large onset about 3 to 4 sec after the theoretical PKP_{BC} arrival. It cannot be a near-source effect, since it is not observed, with the same time delay, at other stations in the network. Unlike the SBF station, such a secondary arrival is not systematically observed at other distance ranges, and a crustal reverberation origin is thus not fully obvious. If

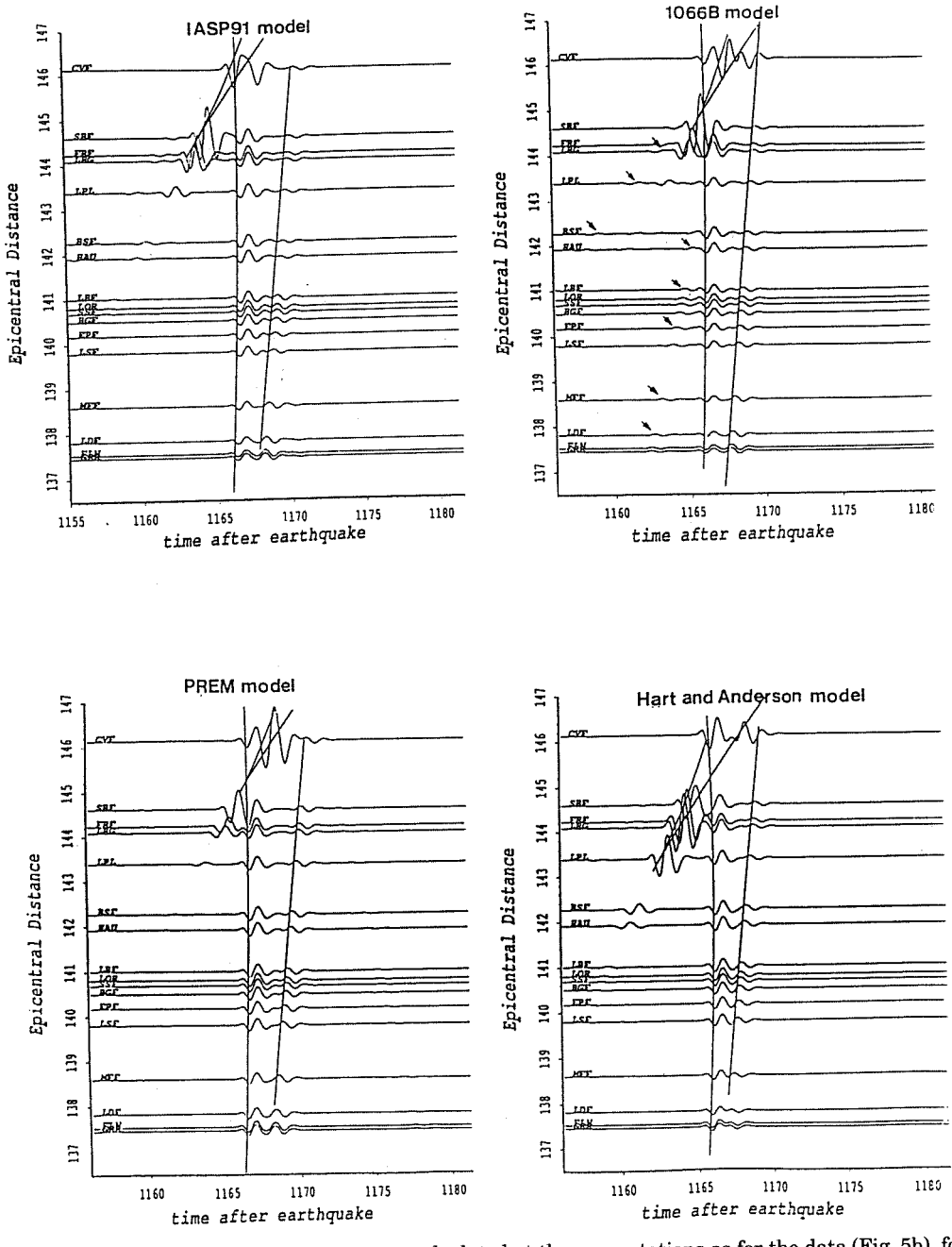

FIG. 6. Synthetic WKBJ seismograms calculated at the same stations as for the data (Fig. 5b), for models IASP91, 1066B, PREM, and Hart and Anderson, respectively. The corresponding theoretical travel-time curves are also displayed. Same set up and scale as in Figure 5b. Spurious artifacts are visible (arrows) on the synthetic seismograms computed for model 1066B.

we attribute it to the PKP_{AB} arrival, the agreement is rather poor. Nevertheless, the time delay between the two *PKP* branches is then inconsistent with the theoretical *PKP* travel times computed for all four Earth models, which predict much smaller time delays at station CVF (Fig. 6). It is further illustrated in Figure 5a, for a Samoa Island earthquake in the South Pacific (Table 1), recorded on the LDG network. The *PKIKP*, PKP_{BC}, and PKP_{AB} wave move-out is clearly visible on the signals. The distance range sampled is 147° to 153°. The theoretical travel-times are computed using the same model (1066B) as in the *bottom* panel, for a 68 km focus depth. The scale is the same for the two panels of Figure 5. Theoretical travel times match the *PKP* wave onsets very well in the *upper* panel (Samoa earthquake), and prolongate exactly into the *PKP* arrival times computed for the *bottom* panel (Mururoa explosions) in the 145° to 147° distance range. The time separation between the two *PKP* branches could thus not be as large as 3 to 4 sec at station CVF, around 146°.

Around 146°, synthetic waveforms become very sensitive to epicentral distance because the two *PKP* branches just begin to separate from each other. To illustrate this, synthetic seismograms have been calculated every 0.1° between 142° and 147°, for the 1066B model (Fig. 7). The waveform agreement at CVF is thus a very good test to discriminate between different Earth structures.

The synthetics computed for the Anderson and Hart model (1976), Figure 6 *bottom right*, are in poor agreement with the data, both on waveforms and amplitudes. It results mainly from the location of the B caustic point, which is computed at too short a distance (143.5°). Large *PKP* amplitudes are produced at stations LPL and LPG, unlike in the data (Fig. 5b). Moreover, the synthetic waveforms poorly match the data stations SBF and CVF because the separation between the two *PKP* branches is much too large.

For the IASP91 model (Kennett and Engdahl, 1991), the agreement is rather poor too. The *B* caustic point is computed at 144.2°. This seems to be too close in distance, as for the Anderson and Hart model, because the PKP amplitude is already large at stations LPL and LPG. However, although it is closer than for the 1066B model, the *PKP* branches are less separated at station CVF, and the synthetic waveforms give a poor match at this station. This shows that the *PKP* amplitude variations near the caustic are governed not only by the position of the *B* caustic point, but also by the acuteness of the focusing effect. The most striking feature of the IASP91 model is perhaps the large separation between the *PKIKP* and *PKP* waves (around 143°), compared with that of model 1066B for instance (Fig. 6 *top left* and *right* panels).

Synthetic seismograms computed for model PREM (Dziewonski and Anderson, 1981) seem to be in closer agreement. However, the *B* caustic point is computed at 144.9°, so that the amplitude at station CVF is too strong, and the two *PKP* branches are not enough separated to match the data (Fig. 5b).

Amplitude Analysis

For the amplitude analysis, 17 explosions have been selected (Table 1), all in the same magnitude range. The change of epicenter location from one blast to another involves shifts of epicentral distances of up to 0.18°, which contributes to the sampling of the caustic.

The 17 blasts have been divided into three groups. (1) The first group, A_1, is a subset of three explosions whose epicenter locations give the shortest epicentral distances. (2) The second, A_2, is a subset of five explosions of the same

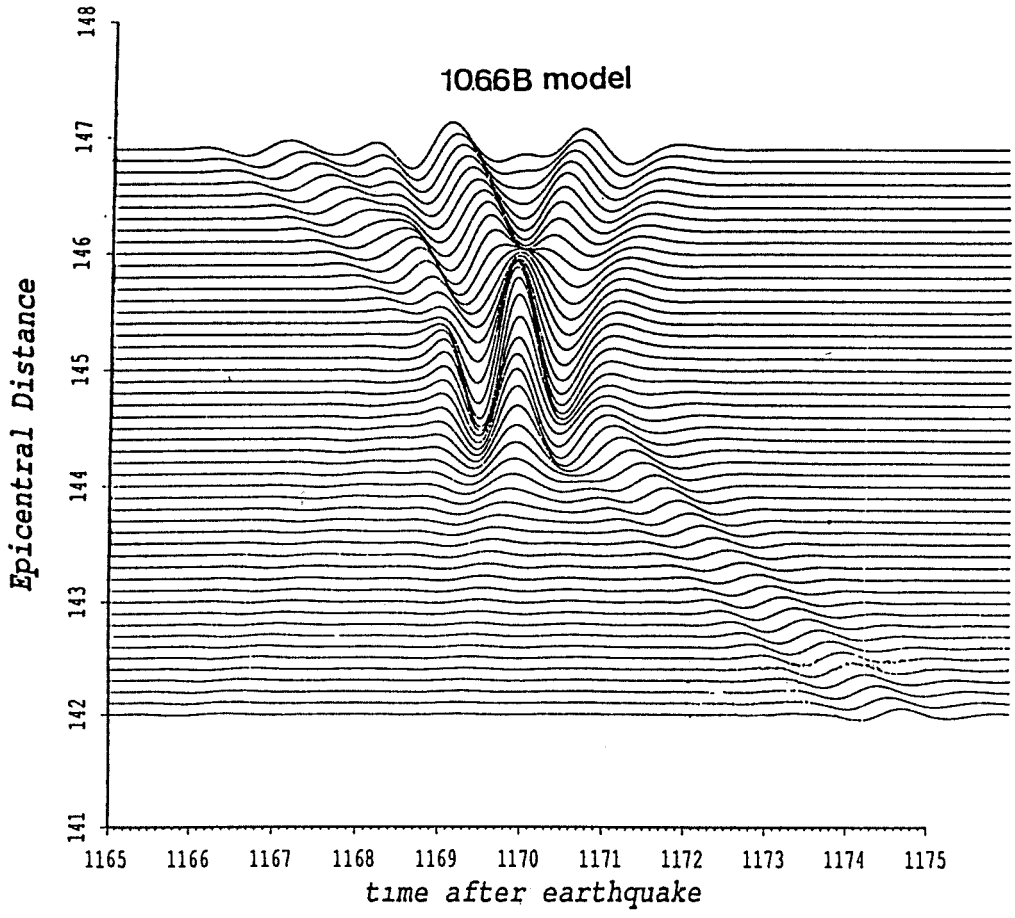

FIG. 7. Theoretical seismograms computed for the 1066B model, every 0.1° from 142° to 147°. They illustrate the waveform and amplitude variations occurring throughout the caustic. Times are reduced using a 3.3 sec/deg slowness.

magnitude (Table 1) and only a few kilometers from each other. The A_2 group is thus treated as a single mean event. The corresponding epicentral distances are the greatest within the set of 17 events. The epicentral distance shifts are 0.14°, 0.16°, and 0.18° between the mean A_2 group event and the three events of group A_1. (3) The third group, A_3, consists of seven blasts of intermediate epicenter locations that give additional amplitude data between 143.5° and 146.2° for stations in the Alps and Provence.

The events of groups A_1 and A_3 are located on the Mururoa atoll, whereas those of group A_2 are located on the Fangataufa atoll.

(1) COMPARISON WITH MASSOT AND ROCARD (1982)

The amplitude versus distance pattern derived by Massot and Rocard (1982) displays very rapid amplitude variations, with interference fringes as narrow as 0.3° (Fig. 1). These data were obtained using two early Mururoa blasts. It is thus interesting to make a similar analysis, with a new set of data, and to compare them with synthetic amplitudes calculated for current Earth models.

The amplitude measurement we use for both data and synthetics is the maximum zero to peak amplitude of the seismograms. Note that Massot and Rocard used a peak to peak amplitude measurement. For the data, we were cautious to attribute the maximum amplitude to direct core wave features (not precursors to the *PKIKP* wave) and around the same feature from one blast to another. The blasts we use have very similar magnitudes (Table 1). Deconvolution from the instrumental LDG response is thus unnecessary. In order to make the events comparable, we opted for relative amplitudes plots. For each blast, the amplitudes plotted in Figures 8a and 8b correspond to amplitudes at a given station divided by a mean amplitude calculated from a subset of 11 stations, in the 139° to 142.5° distance range. In this range, the position of the maximum amplitude corresponds to the *PKIKP*-wave arrival, in which the theoretical amplitude is almost constant (Fig. 4). The same treatment is applied to the synthetics, allowing a valuable comparison between synthetic calculations and data.

Figure 8a shows that the amplitude of the data is roughly constant between 137° and 143°, as expected from the WKBJ calculations for the *PKIKP* wave in the same distance range (see above in text). Because of the scatter in the data, it is not possible to detect a *PKIKP* + *PKiKP* interaction near 137°, where the two waves are very close to each other (Fig. 5b). The data display a steep increase of amplitude near 144°, but *no oscillation is visible between* 144° *and* 144.7°, as in Massot and Rocard (Fig. 1). Because the mean event of group *A*2 (star) has global epicentral distance shifts of 0.14° (small cross), 0.16° (filled square), and 0.18° (large cross) compared with the three events of group *A*1, we can use this to check if the amplitude variations observe such rapid oscillations with distance. For example, the positions of the *FRF and SBF stations* would correspond to *a hole of the oscillatory pattern of Figure* 1, *for the events of group A*1, and to *a maximum for the mean event of group A*2. Our data rather show a *slight increase of the amplitudes at these stations between the two groups of data.* Moreover, because the event of group A2 is a stacked event, star points amplitudes in Figure 8a are thus more reliable. The slight increase of amplitude from one group to another is a good illustration of the rate of increase of the amplitude of the *PKP* waves within the rising part of the caustic.

Our synthetic calculations support, as well, the existence of a single *PKP* peak pattern through the caustic. This peak is only modulated by the simultaneous arrival of the *PKIKP* wave near 145°, because of the large amplitude ratio between the *PKP* and *PKIKP* waves in this distance range (Fig. 4). The reason why the separation of the two *PKP* branches beyond 145° does not produce a more complex oscillatory amplitude pattern, as in Figure 1, is rather straightforward: the dominant period of the synthetic signals is around 1 sec, as in the data; to interfere destructively, the two *PKP* waves must be separated by half a period. The *PKP* travel-time tables computed for the IASP91 model, for instance, show that such a phase shift is not observed at a distance closer than 146°, *at this period.* This is confirmed by the theoretical amplitude curve computed for the IASP91 model, using a complex source time-history (Fig. 8a). The source time function is a Müller–Murphy (1971) wavelet convolved by a 3.5 sec long 1 Hz cosine wavelet. This should match more closely the source time wavelet observed for explosions of larger magnitude, as those used by Massot and Rocard (1982). Compared with the theoretical curve for model IASP91 using a simple Müller and Murphy source function, amplitudes are very much alike,

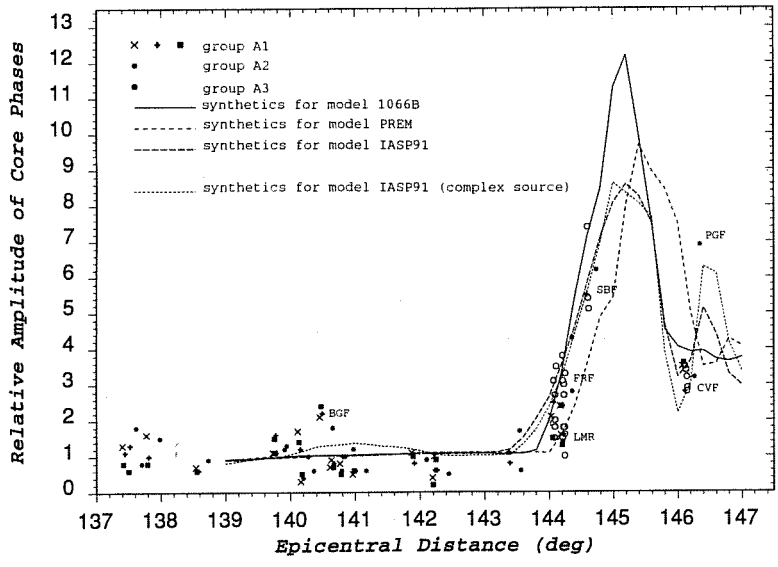

(a)

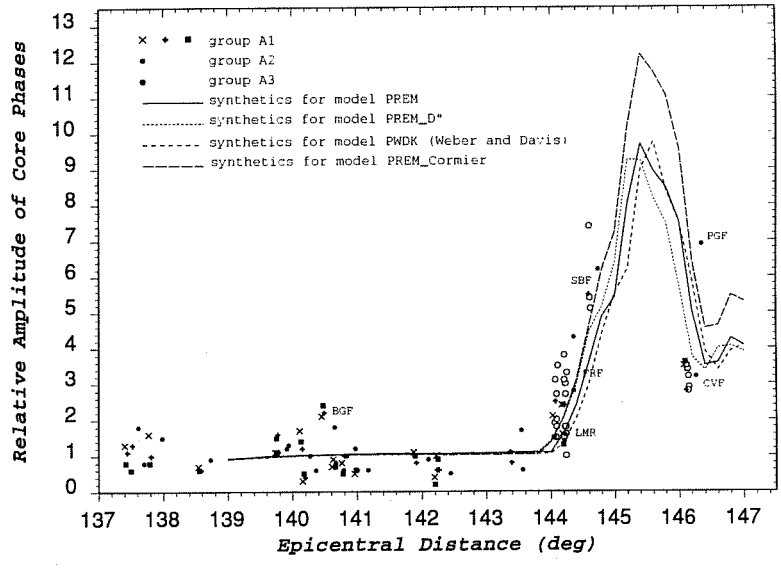

(b)

FIG. 8. Relative amplitude versus distance curves between 137° and 147°. The symbols used for the theoretical curves and for the data of the A_1, A_2, and A_3 groups are indicated in the *top left* part of the figure. Amplitudes are relative to a mean amplitude calculated between 139° and 142.5°. The points for group A_2 (stars) are relative amplitudes for a "mean" or stacked event obtained at each station by the summation of the five events of the group. The epicentral distances are corrected for the Earth's ellipticity.

(a) Data, and theoretical curves for spherical models 1066B, PREM, and IASP91. For the latter, a second curve is shown, where a complex source history is obtained by convolving the Müller–Murphy source with a 1 Hz, 3.5-sec duration, cosine wavelet.

(b) Data, and theoretical curves for model PREM and recent revised structures of D″ and of the core. PREM_D″ is the same model as PREM, except in D″ where a 3% *P*-velocity discontinuity is present 290 km above the cmb. PWDK (Weber and Davis, 1990) is the same model as PREM_D″, except that the cmb radius is that of Jeffreys–Bullen (9 km deeper than in PREM). PREM_Cormier has the *P* velocity of PREM but the $Q(r)$ model of Cormier (1981) in the inner core.

except around 146°, where the secondary interference peak is much more pronounced. The width of the caustic peak is thus independent of the source duration, *at a given frequency*.

The 1066B model amplitude curve is in close agreement with our data, as well as that of the IASP91 model, unlike in the waveform analysis. The position of the *B* caustic point, as well as the rate of the amplitude variations throughout the caustic are well reproduced. The synthetic amplitudes fall to about 3 to 4 at 146.2°, in close agreement with the cluster of observed amplitudes at station CVF.

For the PREM model, the position of the B caustic point seems to be a bit too far to match closely the data around 144°. The disagreement is more obvious at 146.2°; the theoretical amplitude is still too large, about 7, to match the amplitudes observed at station CVF. On the contrary, for the Anderson and Hart model, the position of the *PKP* caustic peak, located around 144°, is much too close to fit the data. The amplitude curve has thus not been displayed in Figure 8a.

For models 1066B and PREM, the relative amplitude at the caustic peak is respectively about 12 and 10 times the mean amplitude around 140°. The halfwidth of the peak is about 1° wide. For these two models, the simultaneous arrival of the *PKIKP* and *PKP* waves occurs right when the PKP waves display a maximum amplitude, so that the caustic peak is only modulated by the interferences. For the model IASP91, the relative amplitude of the peak is only 8.5, but its halfwidth is wider (about 1.5°). The agreement with amplitudes at station CVF is particularly good. Unlike PREM and 1066B models, the interferences between the *PKIKP* and *PKP* waves produce a pronounced secondary peak, around 146.5°. This results from the large separation observed between the *PKIKP* and *PKP* branches for this model (Fig. 6). The interferences occur thus in the descending part of the *PKP* caustic peak, where the amplitude ratio of the *PKP* and *PKIKP* waves is weaker. This is an interesting feature to discriminate between different core structures.

Station Amplitude Anomalies

Unlike for travel-times, it has not been possible to derive station amplitude corrections. Such anomalies are likely to depend on distance, azimuth, and frequency. To derive amplitude corrections, a distance range where the amplitude of the waves is almost constant is required, as in the 139° to 142.5° range for the *PKIKP* wave. The existence of a positive amplitude anomaly is thus clearly shown for the BGF station (Fig. 8a). However, the rapid variation of such anomalies is illustrated in Figure 5a, where the amplitude at station BGF is quite normal. Unfortunately, no seismic region has the appropriate location to make epicentral distances at stations in the Alps, Provence, and Corsica match the 139° to 142.5° range. Nevertheless, some *relative* anomalies are observed in Figure 8a, for couples of stations at the same distance from Mururoa. For instance, the amplitude at station FRF is about twice that at station LMR. This is the same for stations PGF and CVF, which are only 0.1° away in distance, although the secondary peak observed for model IASP91 might account for part of it. Together with the amplitude anomaly of station BGF, this gives a factor of 2 estimate for the station statics of our short period amplitudes.

The scatter of amplitudes may explain part of the discrepancies observed between the amplitude versus distance pattern of Massot and Rocard (1982)

(Fig. 1) and ours (Fig. 8a). The SPF station, in Figure 1, was very close to the current location of the FRF station. Whereas Massot and Rocard fit the amplitudes at the LMR and SPF stations with an oscillatory pattern, we rather interpret the factor of 2 between the mean amplitudes of the two clusters of points at stations LMR and FRF as a result of the scatter of amplitudes of short-period data. Nevertheless, the global amplitude pattern of our data set is in good agreement with the theoretical calculations. In Figure 1, the amplitudes display a smooth increase between 142° and 143.5°, whereas a roughly constant amplitude is observed in Figure 8a. In this distance range, we attribute the maximum amplitude of seismograms to the direct *PKIKP* wave, whereas Massot and Rocard (1982) attribute it to the *PKIKP* precursors. A last discrepancy is observed around 145°, between amplitudes of Figure 1 and our synthetic calculations. Whereas a theoretical broad caustic peak is predicted (Fig. 8a), the amplitude at station Parzanico is quite weak (about the same as at station CVF). We have no obvious explanation for such a discrepancy. Amplitude points between 145° and 146° were obtained using mobile LDG instruments in Italy, for a single blast. Supplementary data are necessary in this distance range. Moreover, the mobile Italian stations were located just south of Lago di Garda, where strong focusing and defocusing effects are expected (Massot and Rocard, 1982).

(2) Comparisons for Revised Earth Structures

As a second step, it is interesting to investigate the effects of locally revised structures of standard Earth models, on the characteristics of the *PKP* caustic. The PREM model is taken as the reference model, in Figure 8b, as in most recent studies. The revised structures mentioned in the Introduction have been tested. Revised structures supporting reduced P velocities in the 100 km outermost core (Lay and Young, 1990) and a constant P velocity in the 150 km above the inner core boundary (Souriau and Poupinet, 1991) produce no noticeable change in the amplitude pattern of model PREM, and are thus not displayed in Figure 8b. Note that the inner core transition zone does not affect *PKP* waves (see raypaths in Fig. 3a). The inner core anelastic model of Cormier (1981) is tested. The amplitude of the *PKIKP* wave is about 20% weaker than for model PREM. Because we are plotting *relative* amplitudes, the PKP caustic peak is 20% higher than with PREM (Fig. 8b). The amplitude at the peak is then as high as for model 1066B (Fig. 8a). Models of the D″ region with a discontinuity at its top are tested too; see also Song and Helmberger (1993). A 3% P-velocity jump 290 km above the core-mantle boundary produces a 0.1° shift of the caustic peak toward shorter distances (Fig. 8b). The synthetic curve is then in closer agreement with the data. This could be a valuable constraint on the structure at the base of the mantle, using waves other than P waves, if more data can be obtained in the 145° to 146° distance range. Finally, the PWDK D″ model of Weber and Davis (1990) is tested. The only difference in the previous D″ model is the depth of the core-mantle boundary (cmb), the radius of the cmb in PWDK is that of the Jeffreys–Bullen model (3471 km) and not that of PREM (3480 km). A shift of 0.25° of the caustic peak is thus observed toward larger distances, compared with the first D″ model curve. The agreement with the data is poorer. Because the B caustic point computed for the PREM model seems to be too far already, this supports rather larger values of the cmb radius. This radius is 3482 km for the IASP91 model and 3485.5 km for the 1066B

model, which are in good agreement with the data (Fig. 8a). However, this cannot fully account for the discrepancies between the different models, in Figure 8a. For example, the cmb radius is almost the same for the IASP91 and PREM models.

The PKP caustic seems to be a rather global feature of Earth models. It is thus not obvious to determine if special zones in the Earth have a pronounced influence on its characteristics.

Conclusion

Using the favorable Mururoa Test Site/LDG network configuration, and the exact knowledge of the explosion source parameters, we have carried out a careful study of the core waves waveform and amplitude variations between 137° and 147°. For the 1066B and IASP91 models, synthetic calculations using the WKBJ method are in good agreement with the data. Our calculations do not support the complex oscillatory amplitude pattern found by Massot and Rocard (1982), and our data are compatible with a single amplitude peak in the 144° to 144.7° distance range. Precise constraints are obtained on the *PKP* caustic, such as the rate of the amplitude variations, the position of the *B* caustic point (144.5° ± 0.5°) for the mean Mururoa-France azimuth and for near-surface events. Various Earth models are tested in theoretical calculations. The PREM model is rather inaccurate to model the *PKP* caustic closely. Models with revised structures produce only slight changes in the characteristics of the caustic, which appears to be a global feature of Earth models. Finally, supplementary data are necessary to better constrain the position of the *PKP* caustic peak, between 144.5° and 144.5°, and to check the existence of a secondary peak near 146°.

Acknowledgments

We are indebted to Chris Chapman for making his WKBJ algorithm available to the community. We thank Annie Souriau for helpful discussions on the subject, Stéphane Gaffet, Thorne Lay, and Donald Helmberger for critical review.

References

Anderson, D. L. and R. S. Hart (1976). An earth model based on free oscillations and body waves, *J. Geophys Res.* **81,** 1461–1475.

Bataille, K. and S. Flatté, 1988). Inhomogeneities near the core-mantle boundary inferred from short-period PKP waves recorded at the global digital seismograph network, *J. Geophys. Res.* **93,** 15,057–15,064.

Baumgardt, D. R., 1989. Evidence for a *P* wave velocity anomaly in D″, *Geophys. Res. Lett.*, **16,** 657–661.

Bertrand, A. E. S. and R. M. Clowes. (1974). Seismic array evidence for a two-layer core transition zone, *Phys. Earth. Planet. Interiors*, **8,** 251–268.

Bullen, K. E., (1949). Compressibility-pressure hypothesis and the Earth's interior, *Monthly Notices Roy Astr. Soc.*, **5,** 355–368.

Chapman, C. H. (1976). A first motion alternative to geometrical ray theory, *Geophys. Res. Lett.*, **3,** 153–156.

Chapman, C. H. (1978). A new method of computing synthetic seismograms, *Geophys. J. R. Astr. Soc.*, **54,** 481–518.

Chapman, C. H. and J. A. Orcutt. (1985). The computation of body wave synthetic seismograms in laterally homogeneous media, *Rev. Geophys.* **23,** 105–163.

Chapman, C. H., J. Y. Chu and D. G. Lyness. (1988). The WKBJ seismogram algorithm, in Seismological Algorithms, Computational Methods and Computer Programs, edited by Doornbos, D., Academic Press, London, 47–76.

Choy, G. L. (1977). Theoretical seismograms of core phases calculated by frequency dependent full-wave theory, and their interpretation, *Geophys. J. R. Astr. Soc.* **51,** 275–312.

Choy, G. L. and V. F. Cormier. (1983). The structure of the inner core inferred from the short-period and broadband GDSN Data, *Geophys. J. R. Astr. Soc.*, **72,** 1–21.

Cormier, V. F. (1981). Short-period PKP phases and the anelastic mechanism of the inner core, physics. *Earth Planet. Interiors*, **24,** 291–301.

Dey-Sarkar, S. K. and C. H. Chapman. (1978). A simple method for the computation of body-wave seismograms, *Bull. Seism. Soc. Am.* **68,** 1577–1593.

Dziewonski, A. M. and D. L. Anderson. (1981). Preliminary reference Earth model, physics. *Earth Planet. Interiors*, **25,** 297–356.

Cummins, P. and L. Johnson. (1988). Synthetic seismograms for an inner core transition of finite thickness, *Geophys. J.*, **94,** 21–34.

Dziewonski, A. M. and D. L. Anderson. (1983). Travel times and station corrections for *P* waves at teleseismic distances, *J. Geophys. Res.* **86,** 3296–3314.

Ergin, K. (1967). Seismic evidence for a new layered structure of the Earth's core, *J. Geophys. Res.* **72,** 3669–3687.

Ergin, K. (1974). Recent observations of the times of core phases, in exploitation of seismograph networks, Noordhoff Leiden, Netherlands, 535–540.

Gaherty, J. B. and T. Lay. (1991). Investigation of laterally heterogeneous shear velocity structure in D″ beneath Eurasia, *J. Geophys. Res.*, **97,** 417–436.

Gilbert, F. and A. M. Dziewonski. (1975). An application of normal mode theory to the retrieval of structural parameters and source mechanisms for seismic structure, *Phil Trans Roy. Soc. London A*, **278,** 187–269.

Gutenberg, B. (1914). Über Erdbebenwellen VIIA Beobachtungen an Registrierungen von Fernbeben in Göttingen und Folgerungen über die Konstitution des Erdkörper, Nachr. dK Ges. dWiss zu Göttingen, Math-Phys. Klasse, 125–177.

Haddon, R. A. W. (1972). Corrugations on the mantle-core boundary or transition layers between inner and outer cores? (abstract), *EOS*, **53,** 600.

Haddon, R. A. W. and J. R. Cleary. (1974). Evidence for scattering of seismic *PKP* waves near the core-mantle boundary, *Phys. Earth. Planet. Interiors*, **8,** 211.

Houard, S., J. P. Massot, J. L. Plantet, and Y. Cansi. (1991). Amplitude des Ondes du Noyau. Partie 1: modélisations par la méthode W.K.B.J., Atomic Energy Agency internal report.

Husebye, E. S., D. W. King, and R. A. W. Haddon. (1976). Precursions to *PKIKP* and seismic waves scattering near the mantle-core boundary, *J. Geophys. Res.*, **81,** 1870–1882.

Jeffreys, H. (1939). The time of core waves, Monthly Notice Roy. Ast. Soc., *Geophys. Suppl.*, **4,** 548–561.

Kennett, B. L. N. (1983). *Seismic Wave Propagation in Stratified Media*, Cambridge University Press, New York.

Kennett, B. L. N. and E. R. Engdahl (1991). Traveltimes for global earthquake location and phase identification, *Geophys. J. Int.* **105,** 429–465.

Lay, T. and D. V. Helmberger. (1983). A lower mantle *S* wave triplication and the shear velocity structure of D″, *Geophys. J. R. Astr. Soc.* **75,** 799–838.

Lay, T. and C. J. Young. (1990). The stably-stratified outermost core revisited, *Geophys. Res. Lett.*, **17,** 2001–2004.

Massot, J. P. and Y. Rocard. (1982). Variation of amplitude of *PKP* from underground explosions in the Southcentral Pacific, *Geophys. Res. Lett.*, **9,** 1211–1214.

Massinon, B. and J. L. Plantet. (1976). A large-aperture network in France: description and some results concerning epicenter location and upper-mantle anomalies, *Phys. Earth Planet. Interiors*, **12,** 118–127.

Müller, and Murphy. (1971). Seismic characteristics of underground nuclear detonations. Part I: seismic spectrum scaling, *Bull. Seism. Soc. Am.* **6,** 1675–1692.

Müller, G. (1973). Amplitude studies of core phases, *J. Geophys. Res.*, **78,** 3469–3490.

Nakanishi, I. (1990). High-frequency waves following *PKP*-C_{diff} at distances greater than 155°, *Geophys. Res. Lett.*, **17,** 639–642.

Richards, P. G. (1976). On the adequacy of plane-wave reflection/transmission coefficients in the analysis of seismic body waves, *Bull. Seism. Soc. Am.*, **66,** 701–717.

Song, X. and D. Helmberger. 193. Effect of velocity structure in D″ on PKP phases, *Geophys. Res. Lett.*, **20,** 285–288.

Souriau, A. and G. Poupinet. (1991). A study of the outermost liquid core using differential travel times of the *SKS*, *SKKS*, and *S3KS* phase, *Phys. Earth Planet. Interiors*, **68,** 183–199.

Souriau, A. and G. Poupinet. (1991). The velocity profile at the base of the liquid core from *PKP*(BC + C_{diff}) data: an argument in favour of radial inhomogeneity, *Geophys. Res. Lett.*, **18,** 2023–2026.

Weber, M. and J. P. Davis. (1990). Evidence for a laterally variable lower mantle structure from *P* and *S* waves, *Geophys. J. Int.*, **102,** 231–255.

Young, C. J. and Lay, T. (1990). Multiple phase analysis of the shear velocity structure in the D″ region beneath Alaska, *J. Geophys. Res.*, **95,** 17385–17402.

DÉPARTEMENT TERRE-ATMOSPHÈRE-OCÉAN
ECOLE NORMALE SUPÉRIEURE
24 RUE LHOMOND
75231 PARIS 05, FRANCE
(S.H., H.C.N)

LABORATOIRE DE DÉTECTION ET DE GÉOPHYSIQUE
B.P12, 91680 BRUYÈRES-LE-CHÂTEL, FRANCE
(J.L.P., J.P.M.)

Manuscript received 26 October 1992